PRIMAL DUAL INTERIOR POINT OPTIMIZATION FOR PENALIZED LEAST SQUARES ESTIMATION OF ABUNDANCE MAPS IN HYPERSPECTRAL IMAGING

S. Moussaoui, J. Idier

L'UNAM Université, Ecole Centrale Nantes
CNRS, IRCCyN (UMR 6597), France

E. Chouzenoux

Université Paris-Est Marne-La-Vallée
IGM (UMR CNRS 8049), France

ABSTRACT

The estimation of abundance maps in hyperspectral imaging (HSI) requires the resolution of an optimization problem subject to non-negativity and sum-to-one constraints. Assuming that the spectral signatures of the image components have been previously determined by an endmember extraction algorithm, we propose here a primal-dual interior point algorithm for the estimation of their fractional abundances using a penalized least squares approach. In comparison with the reference method FCLS, our algorithm has the advantage of a reduced computational cost, especially in the context of large scale images and allows to deal with a penalized criterion favoring the spatial smoothness of abundance maps. The performances of the proposed approach are discussed with the help of a synthetic HSI example.

Index Terms— Spectral unmixing, non-negativity, sum-to-one, interior point optimization, primal-dual algorithm.

1. INTRODUCTION

The main goal of any hyperspectral image (HSI) analysis method is the identification of the observed scene components (endmembers) from their spectral signatures and the determination of their fractional abundances inside each pixel area [1]. In a supervised approach, the endmember spectra are supposed to be known from a spectral library or estimated using an endmember extraction algorithm [2]. Thus, the remaining step of spectral unmixing is the estimation of the fractional abundances.

Let us consider N pixels of a hyperspectral image acquired in L spectral bands and assume a linear mixing model. Thus, each observed spectrum $\boldsymbol{y}_n \in \mathbb{R}^{L\times 1}$ in the n-th pixel can be explained as a linear combination of P endmember spectra and corrupted by an additive noise $\boldsymbol{\epsilon}_n$,

$$\boldsymbol{y}_n = \boldsymbol{S}\,\boldsymbol{a}_n + \boldsymbol{\epsilon}_n, \tag{1}$$

where $\boldsymbol{S}_p = (\boldsymbol{s}_1, \ldots, \boldsymbol{s}_P)$ contains the endmember spectra and $\boldsymbol{a}_n = [a_{n,1}, \ldots, a_{n,P}]^{\mathrm{t}}$ is the vector of endmember abundances in the n-Th. pixel. The abundance vectors $\{\boldsymbol{a}_n; \forall n = 1, \ldots, N\}$, should satisfy the non-negativity constriant and may also be constrained to sum-to-one,

$$a_{n,p} \geqslant 0, \quad \forall\, p = 1, \ldots, P, \tag{2a}$$

$$\sum_{p=1}^{P} a_{n,p} = 1. \tag{2b}$$

Using matrix notations, the mixing model is rewritten as,

$$\boldsymbol{Y} = \boldsymbol{S}\,\boldsymbol{A} + \boldsymbol{E}, \tag{3}$$

where $\boldsymbol{Y} \in \mathbb{R}^{L\times N}$ is the observation data matrix, $\boldsymbol{S} \in \mathbb{R}^{L\times P}$ the spectral signatures, $\boldsymbol{A} \in \mathbb{R}^{P\times N}$ the fractional abundance matrix and $\boldsymbol{E} \in \mathbb{R}^{L\times N}$ the measurement noise. Available algorithms for solving the inverse problem of estimating $\boldsymbol{A}$ from $\boldsymbol{Y}$ and $\boldsymbol{S}$ consist on the minimizing a least squares objective function under constraint (2a) (NNLS [3], *non-negative least squares*) or (2b) (SCLS [4], *sum-to-one constrained least squares*) or under both constraints (2a) and (2b) (FCLS [5], *fully constrained least squares*). In [6], a Bayesian inference algorithm incorporating constraints (2a) and (2b) is proposed. It is based on Monte Carlo Markov chain methods and offers the advantage of estimating the number of components. However, all the mentioned methods suffer from a significant increase of the computation time in the case of large data sets (in terms of image size or number of components).

We propose in this paper a spectral unmixing algorithm based on penalized least squares estimation and interior point optimization [7, 8] using a primal-dual approach [9]. While the penalized least squares approach aims at introducing a prior knowledge on the abundance maps, the interior point optimization approach allows to minimize any convex objective function under equality (sum-to-one) and inequality (non-negativity) constraints. Therefore, it can be applied for the minimization of the least squares criterion augmented by a regularization term allowing to introduce a spatial smoothing of the abundance maps. From the numerical optimization point of view, the interior point algorithm needs to a solve a large linear system of equations at each iterate. We will show that an approximate resolution of such system using a preconditioned bi-conjugate gradient [10] reduces significantly the computation cost without altering the unmixing performances.

2. PRIMAL-DUAL OPTIMIZATION FOR ABUNDANCE MAPS ESTIMATION

The estimation of $\boldsymbol{A}$ is firstly formulated as the minimization of a convex criterion $F(\cdot)$,

$$\min_{\boldsymbol{A}\in\mathbb{R}^{P\times N}} F(\boldsymbol{A}) \quad \text{s.t.} \quad \text{(2a) and (2b)}. \tag{4}$$

An interior point algorithm based on a primal-dual approach is then used for the resolution. While the image pixels can be unmixed separately in the least squares criterion case, the optimization algorithm should be applied jointly to all the pixels in the case of a criterion accounting for spatial dependencies between pixels.

2.1. Criterion formulation

The criterion $F(\cdot)$ results from the statistical modeling of the observation process and the sought abundance maps. A usual approach is

to assume $F(\cdot)$ as the least squares criterion [4],

$$F(\boldsymbol{A}) = \frac{1}{2}\|\boldsymbol{Y} - \boldsymbol{S}\boldsymbol{A}\|_F^2, \tag{5}$$

where $\|\cdot\|_F$ represents the Frobenius norm. A penalization criterion $R(\cdot)$, can also be considered to get a solution where the abundance maps presents some spatial regularity. For example,

$$R(\boldsymbol{A}) = \sum_{p=1}^{P} \varphi\big(\boldsymbol{\Delta}\boldsymbol{a}_p\big), \tag{6}$$

where $\boldsymbol{\Delta}$ represents the gradient operator and φ a regularization function. A quadratic (ℓ_2) function can be used for a denosing purpose, but a half-quadratic ($\ell_2 - \ell_1$) regularization function would be preferred to preserve the image edges [11]. Finally, the composite criterion takes the form,

$$F(\boldsymbol{A}) = \frac{1}{2}\|\boldsymbol{Y} - \boldsymbol{S}\boldsymbol{A}\|_F^2 + \beta\, R(\boldsymbol{A}), \tag{7}$$

where β is the regularization weight.

2.2. Accounting for the sum-to-one constraint

As suggested by [9], the equality constraint (2b) can be implicitly handled by introducing a reparametrization so that (4) is reduced to an inequality constrained problem. For each initial vector $\boldsymbol{a}^{(1)}$ satisfying the equality constraint (2b), the transformed vector $\boldsymbol{a} = \boldsymbol{a}^{(1)} + \boldsymbol{Z}\boldsymbol{c}$, where $\boldsymbol{c}_n \in \mathbb{R}^{P-1}$, also satisfies the sum-to-one constraint if the columns of matrix $\boldsymbol{Z} \in \mathbb{R}^{P\times P-1}$ are formed from the null space of $\boldsymbol{1}_{1\times P}$. In our case, such matrix can be defined by,

$$Z_{ij} = \begin{cases} 1 & \text{if} \quad i = j, \\ -1 & \text{if} \quad i = j+1, \\ 0 & \text{otherwise.} \end{cases} \tag{8}$$

Thus, problem (4) is rewritten as

$$\min_{\boldsymbol{C}\in\mathbb{R}^{(P-1)\times N}} F\big(\boldsymbol{A}^{(1)} + \boldsymbol{Z}\boldsymbol{C}\big), \tag{9}$$

subject to $\boldsymbol{Z}\boldsymbol{c}_n + \boldsymbol{a}_n^{(1)} \geqslant 0$, $\forall n = 1, \ldots, N$. By introducing the operator $\boldsymbol{m} = \mathrm{vect}\big(\boldsymbol{M}\big)$ which corresponds to the transformation of a matrix $\boldsymbol{M}$ to a vector $\boldsymbol{m}$ in the lexicographic order, the problem also reads

$$\min_{\boldsymbol{c}\in\mathbb{R}^{(P-1)N}} \Phi(\boldsymbol{c}) \triangleq F(\boldsymbol{A}^{(1)} + \boldsymbol{Z}\boldsymbol{C}) \quad \text{s. t.} \quad \boldsymbol{T}\boldsymbol{c} + \boldsymbol{t} \geqslant \boldsymbol{0}, \tag{10}$$

where $\boldsymbol{c} = \mathrm{vect}(\boldsymbol{C})$ and $\boldsymbol{t} = \mathrm{vect}(\boldsymbol{A}^{(1)})$. The matrix $\boldsymbol{T}$ equals to $\boldsymbol{I}_N \otimes \boldsymbol{Z}$ where $\otimes$ is the Kronecker product and $\boldsymbol{I}_N$ the $N \times N$ identity matrix.

2.3. Primal-dual interior point optimization

The main feature of interior point optimization is to keep the solution inside the feasible domain. In fact, at each iteration, the constraint fulfillment is ensured by adding a logarithmic barrier function making the criterion unbounded at the boundary of the feasible solution domain [7]. The primal-dual approach consists in jointly estimating $\boldsymbol{c}$, and their associated Lagrange multipliers $\boldsymbol{\lambda}$ thought the resolution of a sequence of optimization problems obtained from perturbed versions of the Karush-Kuhn-Tucker (KKT) optimality conditions:

$$\begin{cases} \bullet\ \nabla\Phi(\boldsymbol{c}) - \boldsymbol{T}^{\mathrm{t}}\boldsymbol{\lambda} = \boldsymbol{0}, & \bullet\ \boldsymbol{\Lambda}(\boldsymbol{T}\boldsymbol{c} + \boldsymbol{t}) = \boldsymbol{\mu}_k, \\ \bullet\ \boldsymbol{T}\boldsymbol{c} + \boldsymbol{t} \geqslant \boldsymbol{0}, & \bullet\ \boldsymbol{\lambda} \geqslant \boldsymbol{0} \end{cases} \tag{11}$$

where $\boldsymbol{\Lambda} = \mathrm{Diag}(\boldsymbol{\lambda})$ and $\boldsymbol{\mu}_k = \mu_k \boldsymbol{1}_{N(P-1)\times 1}$ is a the sequence of perturbation parameters $\{\mu_k\}$ converging to 0 when k tends to $+\infty$. At each iteration k of the primal-dual algorithm, $\boldsymbol{c}_{k+1}$ and $\boldsymbol{\lambda}_{k+1}$ are firstly calculated from the KKT conditions and the perturbation parameter μ_{k+1} is then updated in order to ensure the algorithm convergence.

In the case of large-scale problems, only an approximate solution of (11) is retained from a Newton algorithm step coupled with a linesearch strategy [8, Chap.11], according to:

$$(\boldsymbol{c}_{k+1}, \boldsymbol{\lambda}_{k+1}) = (\boldsymbol{c}_k + \alpha_k \boldsymbol{d}_k^c, \boldsymbol{\lambda}_k + \alpha_k \boldsymbol{d}_k^\lambda). \tag{12}$$

Primal-dual directions. The directions $(\boldsymbol{d}_k^c, \boldsymbol{d}_k^\lambda)$ are obtained from

$$\begin{bmatrix} \nabla^2\Phi(\boldsymbol{c}_k) & -\boldsymbol{T}^{\mathrm{t}} \\ \boldsymbol{\Lambda}_k\boldsymbol{T} & \mathrm{Diag}(\boldsymbol{T}\boldsymbol{c}_k + \boldsymbol{t}) \end{bmatrix} \begin{bmatrix} \boldsymbol{d}_k^c \\ \boldsymbol{d}_k^\lambda \end{bmatrix} = \begin{bmatrix} \boldsymbol{T}^{\mathrm{t}}\boldsymbol{\lambda}_k - \nabla\Phi(\boldsymbol{c}_k) \\ \boldsymbol{\mu}_k - \boldsymbol{\Lambda}_k(\boldsymbol{T}\boldsymbol{c}_k + \boldsymbol{t}) \end{bmatrix}$$

where $\nabla\Phi(\cdot)$ and $\nabla^2\Phi(\cdot)$ are, respectively, the gradient and the Hessian of criterion $\Phi(\cdot)$, given in (10). In the case of criterion (7), derivatives calculation yield,

$$\nabla\Phi(\boldsymbol{c}) = \mathrm{vect}\left(-\boldsymbol{Z}^{\mathrm{t}}\boldsymbol{S}^{\mathrm{t}}(\tilde{\boldsymbol{Y}} - \boldsymbol{S}\boldsymbol{Z}\boldsymbol{C})\right) + \beta\, \boldsymbol{D}^{\mathrm{t}}\dot{\varphi}\Big(\boldsymbol{D}\,\boldsymbol{c} + \boldsymbol{d}^{(1)}\Big)$$

$$\nabla^2\Phi(\boldsymbol{c}) = \boldsymbol{I}_N \otimes (\boldsymbol{Z}^{\mathrm{t}}\boldsymbol{S}^{\mathrm{t}}\boldsymbol{S}\boldsymbol{Z}) + \beta\, \boldsymbol{D}^{\mathrm{t}}\mathrm{Diag}\left(\ddot{\varphi}\Big(\boldsymbol{D}\,\boldsymbol{c} + \boldsymbol{d}^{(1)}\Big)\right)\boldsymbol{D},$$

where $\tilde{\boldsymbol{Y}} = \boldsymbol{Y} - \boldsymbol{S}\boldsymbol{A}^{(1)}$, $\dot{\varphi}$ and $\ddot{\varphi}$ stand, respectively, for the first and the second derivatives of φ, $\boldsymbol{D} = (\boldsymbol{\Delta} \otimes \boldsymbol{Z})$ and $\boldsymbol{d}^{(1)} = \mathrm{vect}\left(A^{(1)}\Delta^{\mathrm{t}}\right)$.

Rather than solving directly this system, [9] propose to make a variable substitution,

$$\boldsymbol{d}_k^\lambda = \mathrm{Diag}(\boldsymbol{T}\boldsymbol{c}_k + \boldsymbol{t})^{-1}\left[\boldsymbol{\mu}_k - \boldsymbol{\Lambda}_k(\boldsymbol{T}\boldsymbol{c}_k + \boldsymbol{t}) - \boldsymbol{\Lambda}_k\boldsymbol{T}\boldsymbol{d}_k^c\right], \tag{13}$$

in order to calculate the primal direction $\boldsymbol{d}_k^c$ from a reduced system

$$\boldsymbol{H}_k\boldsymbol{d}_k^c = \boldsymbol{T}^{\mathrm{t}}\mathrm{Diag}(\boldsymbol{T}\boldsymbol{c}_k + \boldsymbol{t})^{-1}\boldsymbol{\mu}_k - \nabla\Phi(\boldsymbol{c}_k) \tag{14}$$

where $\boldsymbol{H}_k = \nabla^2\Phi(\boldsymbol{c}_k) + \boldsymbol{T}^{\mathrm{t}}\mathrm{Diag}(\boldsymbol{T}\boldsymbol{c}_k + \boldsymbol{t})^{-1}\boldsymbol{\Lambda}_k\boldsymbol{T}$.

In order to reduce the computation cost, we also propose to perform an approximate resolution of this system using a preconditioned bi-conjudate gradient algorithm [10]. The preconditioning is based on an incomplete LU factorization of matrix $\boldsymbol{H}_k$. Finally (13) is used to calculate the dual direction $\boldsymbol{d}_k^\lambda$.

Linesearch. The stepsize value α_k should be chosen to ensure the convergence of the algorithm and the fulfillment of the inequalities of the pertubed KKT system (11). The employed condition requests a sufficient decrease of the primal-dual merit function $\Psi_\mu(\boldsymbol{a}, \boldsymbol{\lambda})$ defined as in [9],

$$\begin{aligned} \Psi_\mu(\boldsymbol{c}, \boldsymbol{\lambda}) = \Phi(\boldsymbol{c}) &- \mu\sum_{i=1}^{NP}\ln([\boldsymbol{T}\boldsymbol{c} + \boldsymbol{t}]_i) \\ &+ \boldsymbol{\lambda}^{\mathrm{t}}(\boldsymbol{T}\boldsymbol{c} + \boldsymbol{t}) - \mu\sum_{i=1}^{NP}\ln(\lambda_i[\boldsymbol{T}\boldsymbol{c} + \boldsymbol{t}]_i). \end{aligned} \tag{15}$$

One can note that this function contains two logarithmic barrier functions associated to the KKT inequalities. The sufficient decrease is assessed using the Armijo condition,

$$\psi_{\mu_k}(\alpha_k) - \psi_{\mu_k}(0) \leqslant \sigma\,\alpha_k\nabla\psi_{\mu_k}(0) \quad \text{with} \quad \sigma \in (0, 1), \tag{16}$$

where $\psi_{\mu_k}(\alpha) = \Psi_{\mu_k}(\boldsymbol{c}_k + \alpha\boldsymbol{d}_k^c, \boldsymbol{\lambda}_k + \alpha\boldsymbol{d}_k^\lambda)$. The stepsize α_k satisfying (16) is obtained by a backtracking algorithm [8].

Perturbation parameter update. The parameter μ_k is updated using the μ-criticity rule [12] defined by:

$$\mu_k = \theta \frac{\delta_k}{NP}, \tag{17}$$

where $\delta_k = (\boldsymbol{T}\boldsymbol{c}_k + \boldsymbol{t})^{\mathrm{t}}\boldsymbol{\lambda}_k$ is the duality gap and $\theta \in (0, 1)$.

Stopping criteria. The main steps of the optimization method leads to algorithm 1. The calculation of the primal and dual direction (inner loop) is controlled by two conditions [9]:

$$\|\boldsymbol{r}^{\text{prim}}_{\mu_k}\|_\infty \leqslant \epsilon^{\text{prim}}_k \text{ and } \|\boldsymbol{r}^{\text{dual}}_{\mu_k}\|_1 / NP \leqslant \epsilon^{\text{dual}}_k, \tag{18}$$

where $\boldsymbol{r}^{\text{prim}}_{\mu_k}(\boldsymbol{c}_k, \boldsymbol{\lambda}_k)$ and $\boldsymbol{r}^{\text{dual}}_{\mu_k}(\boldsymbol{c}_k, \boldsymbol{\lambda}_k)$ are the primal and dual residuals. $\epsilon^{\text{prim}}_k = \eta^{\text{prim}}\mu_k$, $\epsilon^{\text{dual}}_k = \eta^{\text{dual}}\mu_k$ where η^{prim} and η^{dual} are two positive parameters. The outer iterations of algorithm 1 are run until the fulfillment of the following condition [8, Chap.11]

$$\mu_k \leqslant \mu_{\min} \quad \text{or} \quad \left(\|\boldsymbol{r}^{\text{prim}}_{\mu_k}\| + \|\boldsymbol{r}^{\text{dual}}_{\mu_k}\|\right) \leqslant \epsilon_0. \tag{19}$$

Initialize $\boldsymbol{\lambda}_0 \geqslant \boldsymbol{0}$ and $\boldsymbol{c}_0$ such that $\boldsymbol{T}\boldsymbol{c}_0 + \boldsymbol{t} > \boldsymbol{0}$
While ((19) is not satisfied) **do**
  While ((18) is not satisfied) **do**
    Calculate $\boldsymbol{d}^c_k$ by solving the system (14)
    Deduce $\boldsymbol{d}^\lambda_k$ from (13)
    Search α_k satisfying (16) by backtracking
    Update $(\boldsymbol{c}_{k+1}, \boldsymbol{\lambda}_{k+1})$ according to (12)
  done
  Define μ_{k+1} according to (17).
done

Algorithm 1: Primal-dual interior point algorithm.

3. EXPERIMENTAL RESULTS

In this section we illustrate the applicability of the interior point primal-dual optimization algorithm 1 to spectral unmixing. We analyze its performances in terms of computation time in the case of least squares and penalized least squares criteria. We also analyze the resulting computation time gain when the primal direction is calculated using few iterations of the bi-conjugate gradient algorithm.

In order to simulate realistic HSI data, we pick up randomly P spectra form the USGS (U.S. Geological Survey) library [13]. This library contains 21 spectra of $L = 224$ spectral bands from 383 nm to 2508 nm. The abundances are simulated as the superposition of $K = 30$ 2D gaussian patterns with random location and variance parameters. These images are then normalized to ensure the sum-to-one constraint.

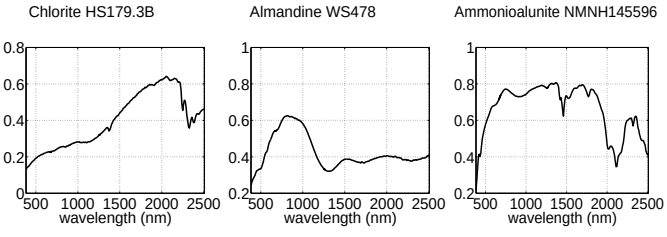

Fig. 1. Example of three endmember spectra (reflectance) taken from the USGS library.

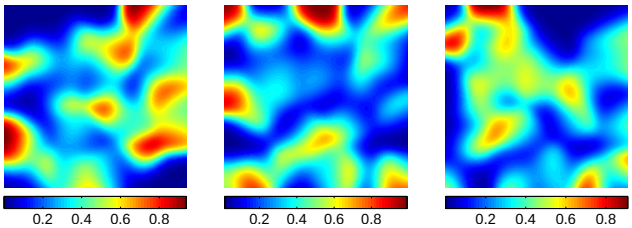

Fig. 2. Example of simulated abundance maps for three components.

Figures 1 and 2 give an example of endmember spectra and abundance maps. A random Gaussian noise is added to each resulting hyspectral image, according to the linear mixing model, in order to get a signal to noise ratio (SNR) of 20 dB. The unmixing algorithms are implemented on Matlab 2007b and the calculations are performed using a MacbookPro having an Intel Core 2 Duo 2.4 GHz processor and 4 GB of RAM (667 MHz).

3.1. Least squares spectral unmixing

In the non penalized case (i.e., $\beta = 0$), the proposed primal-dual optimization approach, referred to as IPLS (for *Interior point least squares*), can be compared with the FCLS algorithm. Different image sizes have been considered (from $N = 64^2$ to 256^2) and the number of endmembers is taken as $P = 3$, 5 or 10. For all the tests (Monte Carlo simulation with 30 realizations), the solutions obtained by the FCLS and the IPLS are very similar. However, as illustrated by figure 3, the proposed approach presents a reduced computation time as compared to FCLS. For example, the gain factor is about 5 for an image of size 256^2 and $P = 10$ endmembers. For this image size, this gain factor is about 7 for $P = 5$ and 11 for $P = 3$.

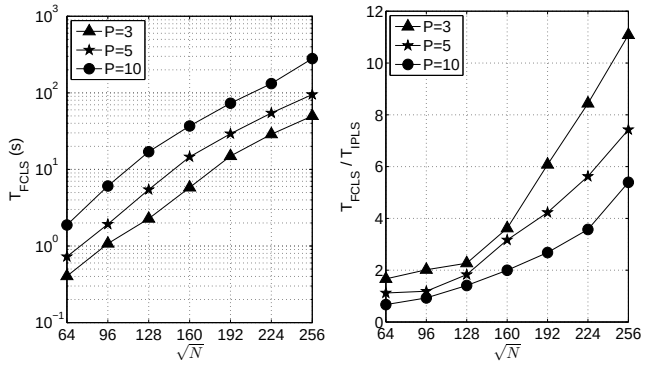

Fig. 3. (**left**) Computation time of the FCLS algorithm and (**right**) gain factor in computation time of the IPLS with respect to the FCLS for different image sizes and number of endmembers.

3.2. Penalized least squares spectral unmixing

A regularization criterion is added by setting $\beta > 0$ and a quadratic function $\varphi(\cdot)$ in (6) in order to account for the spatial smoothness of the abundance maps. In this situation, only the proposed primal-dual algorithm, referred to as IPPLS (for *Interior point penalized least squares*), can be applied. The discussion concerns the influence of an approximate resolution of the primal system (14) on the computation time of the algorithm. Once again, for all the tests (Monte

Carlo simulation with 30 realizations), the results were very similar in terms of final criterion value and obtained solution. As shown in figure 4, the approximate calculation of the primal direction allows to reduce significantly the computation time of the algorithm.

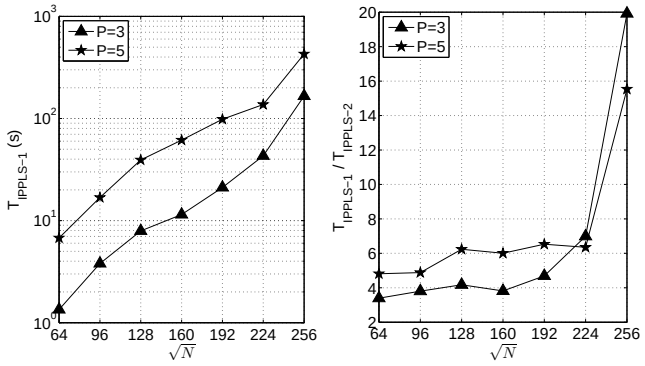

Fig. 4. (**left**) Computation time of the IPPLS-1 algorithm with exact resolution of (14) and (**right**) gain factor of computation time when only an approximate resolution of (14) is performed (IPPLS-2).

3.3. Effect of the noise level

Table 1 presents the obtained results of FCLS, IPLS and IPPLS algorithms in terms of estimated abundance maps quality and computation time for different noise levels.The number of endmembers is set to $P = 5$ and the image size to $N = 256^2$ pixels. In this experiments, the endmembers have been estimated using the VCA method [14]. Finally, the quality of the estimated abundance maps is assessed using the normalized mean square error

$$\text{NMSE}(\%) = \frac{100}{P} \sum_{p=1}^{P} \left(\|\boldsymbol{a}_p - \hat{\boldsymbol{a}}_p\|^2 / \|\boldsymbol{a}_p\|^2 \right), \qquad (20)$$

which measures the dissimilarity between the reference abundances $\boldsymbol{a}_p$ and the estimated ones $\hat{\boldsymbol{a}}_p$. The regularization parameter β is set to 0.1 in order to minimize this error in the case of penalized least squares estimation. On can note that adding the regularization criterion leads to better results as compared to the non penalized least squares case. This enhancement is more significant when the noise level increases. On the other hand, thanks to the approximate resolution of (14), the penalized approach only increases moderately the computation time of the algorithm.

Method	SNR (dB)	20	15	10	5
FCLS	Time (sec.)	91.12	91.19	92.29	92.80
	NMSE (%)	0.18	0.46	1.34	3.64
IPLS	Time (sec.)	10.56	10.63	10.85	10.86
	NMSE (%)	0.18	0.46	1.33	3.63
IPPLS	Time (sec.)	20.20	20.39	20.43	20.45
	NMSE (%)	0.08	0.23	0.68	2.01

Table 1. Computation time and abundance estimation errors of the unmixing algorithms for $P = 5$ and $N = 256^2$.

4. CONCLUSION

We have proposed in this paper a spectral unmixing algorithm allowing to estimate the abundance maps using a primal dual interior point optimization. The main feature of the proposed optimization approach is to fully satisfy the non-negativity and sum-to-one constraint. The second advantage is the possibility to minimize a general criterion including a spatial information on the sought abundances. Future studies will be directed at analyzing the theoretical convergence of the proposed algorithm and its application to the case of non-linear mixing models.

5. REFERENCES

[1] J. R. Scott, *Remote Sensing: The Image Chain Approach*, New York: Oxford Univ. Press, 1997.

[2] M. Parente and A. Plaza, "Survey of geometric and statistical unmixing algorithms for hyperspectral images," in *Proc. of WHISPERS*, Reykjavik, Iceland, June 2010.

[3] C. L. Lawson and R. J. Hanson, *Solving Least-Squares Problems*, Prentice-Hall, Englewood Cliffs, New Jersey, 1974.

[4] J. J. Settle and N. A. Drake, "Linear mixing and the estimation of ground cover proportions," *Int. J. Remote Sens.*, vol. 14, no. 6, pp. 1159–1177, 1993.

[5] D. C. Heinz and C.-I. Chang, "Fully constrained least squares linear spectral mixture analysis method for material quantification in hyperspectral imagery," *IEEE Trans. Geosci. Remote Sensing*, vol. 39, no. 3, pp. 529 –545, 2001.

[6] N. Dobigeon, J.-Y. Tourneret, and C.-I Chang, "Semi-supervised linear spectral unmixing using a hierarchical Bayesian model for hyperspectral imagery," *IEEE Trans. Signal Process.*, vol. 56, no. 7, pp. 2684–2695, 2008.

[7] M. H. Wright, "Interior methods for constrained optimization," in *Acta Numerica 1992*, pp. 341–407. Cambridge University Press, 1991.

[8] S. Boyd and L. Vandenberghe, *Convex Optimization*, Cambridge University Press, New York, 1st edition, 2004.

[9] P. Armand, J. C. Gilbert, and S. Jan-Jégou, "A feasible BFGS interior point algorithm for solving strongly convex minimization problems," *SIAM J. Optim.*, vol. 11, pp. 199–222, 2000.

[10] H. A. Van der Vorst, "BI-CGSTAB: a fast and smoothly converging variant of BI-CG for the solution of nonsymmetric linear systems," *SIAM J. Sci. Comput.*, vol. 13, pp. 631–644, March 1992.

[11] J. Idier, "Convex half-quadratic criteria and interacting auxiliary variables for image restoration," *IEEE Trans. Image Process.*, vol. 10, no. 7, pp. 1001–1009, 2001.

[12] A. S. El-Bakry, R. A. Tapia, T. Tsuchiya, and Y. Zhang, "On the formulation and theory of the newton interior-point method for nonlinear programming," *J. Optim. Theory Appl.*, vol. 89, pp. 507–541, June 1996.

[13] R. N. Clark, G. A. Swayze, A. Gallagher, T. V. King, and W. M. Calvin, "The U.S. geological survey digital spectral library: version 1: 0.2 to 3.0 μm," *U.S. Geol. Surv., Denver, CO, Open File Rep. 93-592*, 1993.

[14] J. M. P. Nascimento and J. M. B. Dias, "Vertex component analysis: a fast algorithm to unmix hyperspectral data," *IEEE Trans. Geosci. Remote Sensing*, vol. 43, no. 4, pp. 898 – 910, April 2005.